Toward the validation of thermochemical models with EAST shock tube radiation measurements

By K. Miki† M. Panesi†, E. Prudencio† AND S. Prudhomme†

Simple thermochemical models describing post-shock flow conditions are developed and subjected to the validation process proposed by Babuška *et al.* (2008) using the latest absolute volumetric radiance data collected at the Electric Arc Shock Tube (EAST) located at the NASA Ames Research Center (ARC). In this validation approach, experimental data is involved only in the calibration of the models, and the decision process is based on the prediction of quantities on interest (QoI's) computed on scenarios that are not necessarily feasible experimentally. Moreover, uncertainties present in the experimental data, as well as those resulting from an incomplete physical model description, are propagated to the QoI's. We investigate two thermochemical models: a one-temperature model under the assumption of thermal equilibrium among all inner modes, and a two-temperature model that is commonly used in the supersonic/hypersonic communities. After statisitically calibrating the uncertain parameters (*inverse* problem) using a Bayesian approach, the statistical *forward* problem is solved in order to examine the robustness of these models. Our results show that the two-temperature model exhibits smaller uncertainties in the prediction of the QoI (the radiative heat flux), than the one-temperature model. However, both models are shown to be invalidated due to unacceptable large uncertainties in the predictions.

1. Introduction

The National Aeronautics and Space Administration (NASA) is presently in the midst of an extensive experimental testing program to support the development of the next generation of space vehicles. Although the design of the Crew Exploration Vehicle (CEV) being developed by NASA to safely return astronauts to Earth is mainly based on Apollo-era concepts, the CEV will be substantially larger than the Apollo capsule. The heating environment experienced during atmospheric entry will therefore be significantly different. One of the most important issues that needs to be addressed in the design of an atmospheric entry vehicle (EV) is thus the accurate calculation of the recession rate of the thermal protection system (TPS), which (the rate) is strongly dependent on the wall heating. In particular, at high reentry speeds, a significant portion of the heating experienced by the spacecraft can be attributed to radiation, which is highly sensitive to the concentration of gas species and distribution of their internal energy level populations. Hence, the correct prediction of the radiative heating is strongly influenced by the model employed for the modeling of the thermal and chemical relaxations. A variety of physical models describing the evolution of the concentration of gas species and the distribution of their internal energy level populations can be found in the literature. In particular, sin-

† Institute for Computational Engineering and Science, The University of Texas at Austin

gle temperature and multi-temperature models (e.g. two-temperature model) have been widely used in the design of the TPS.

In the case of single-temperature models, the physico-chemical properties of the airflow are obtained through the shock layer by assuming that, for all species, the population of each internal (rotational, vibrational, or electronic) energy mode follows a Maxwell-Boltzmann distribution at a common temperature and the chemical relaxation is modeled using a macroscopic kinetic rate. Thus, as opposed to the multi-temperature models, the single temperature model is based on the assumption that the internal energy modes quickly thermalize reaching equilibrium at a common temperature. Multi-temperature models are expected to be more accurate than single-temperature ones in that they allow for the thermal non-equilibrium effects to be accounted for. Indeed, in the latter case, the population of each internal energy mode follows for each species a Maxwell-Boltzmann distribution at a specific temperature (rotational T_r, vibrational T_v, and electronic T_e). Moreover, for the chemical kinetics model, macroscopic rate coefficients are assumed to depend on an empirical temperature expressed as a function of the different temperatures in the flow.

Predictions provided by these physical models are inherently uncertain due to the limited state of our knowledge, the lack of experimental data at the specific flight conditions, and the complexity of the physics involved. The single- and two-temperature models considered here may provide a crude approximation of physico-chemical processes occurring in high-temperatures gases and involve model parameters that need to be calibrated and whose uncertainties have to be quantified. In this work, for the two classes of models studied, we treat the parameters as random variables, calibrate them and propagate their uncertainties to the predicted QoI's.

Classical processes for model validation in science are usually related to data fitting: the closer the values computed by a model are to values measured in experiments, the better the model is. Unfortunately, it often happens that observations from experiments are not directly related to the final quantity of interest (QoI, e.g. the radiative flux) or simply not available for the scenarios or conditions in which the model will be used for prediction purposes. In this case, it may not be possible to infer that a model that predicts well experimental observations can also accurately estimate a QoI. We thus believe that the propagation of uncertainties to the final QoI does constitute an important step in the validation process of a model. The methodology for model validation proposed at the PECOS center involves a probabilistic approach for the calibration of uncertain model parameters and the quantification of uncertainty associated with specific model predictions. The use of experimental data is of course necessary for the calibration of parameters and expert opinion is usually required for the interpretation of the results and decision-making; i.e. a model is deemed invalid if, following the validation process, one considers that the model is unable to provide reliable predictions of specific QoI's at specific prediction scenarios; if otherwise, the model is said to be not invalidated.

The inverse problem is solved for the model parameters using a Bayesian statistical approach. The solutions of the inverse problem are given in terms of posterior probability density functions (pdf's). Experimental data used for the calibration of the parameters are obtained from Electric Arc Shock Tube (EAST) experiments performed at NASA. By Bayes' theorem, *posterior* pdf's are computed from *likelihood functions* and *prior* pdf's. Likelihood functions describe the probability that the model predicts the observed data for given values of the parameters. The prior pdf for each parameter is constructed based on careful consideration of the existing information about the parameter. Calculation

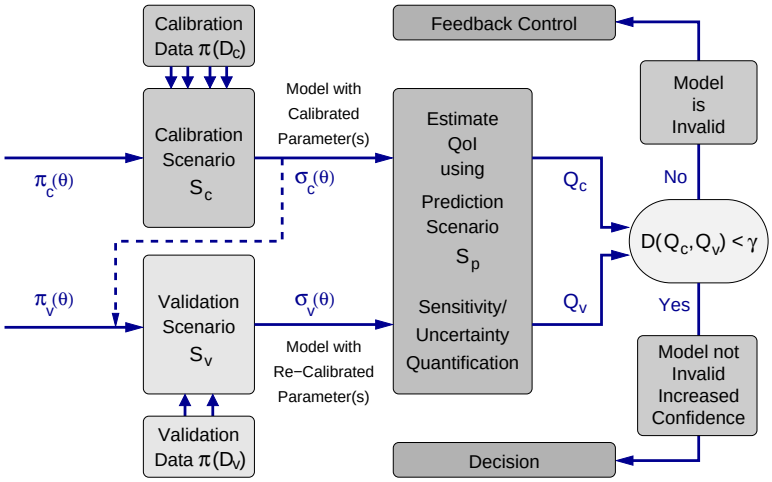

FIGURE 1. Flowchart of the calibration, validation, and prediction processes.

of the posterior pdf's for some uncertain parameters of the single- and two-temperature models is a primary focus of this study.

The validation process to be used in this report is discussed in Section 2, the thermochemical models to simulate post-shock flow conditions are introduced in Section 3, and the experimental data used for the calibration of these models is described in Section 4. Finally, results from the validation procedure are given in Section 5, and concluding remarks are provided in Section 6.

2. Validation Process

The contemporary view of predictive computational modeling for physical events presumes that observational data used in the calibration and validation of models is acquired for simple scenarios of the theory. In addition, one has to consider yet another model scenario, the most complete one and here denoted S_p, for which one hopes to predict the ultimate QoI with a model that survives the validation process.

We briefly describe below the calibration, validation, and prediction processes in the abstract manner presented in Fig. 1. Let us introduce an abstract model problem that consists on finding the solution $u(\theta, S)$ such that

$$\mathcal{A}\left(\theta, S, u(\theta, S)\right) = 0 \tag{2.1}$$

where $\mathcal{A}$ is an operator representing the theory, θ the model parameters, and S some possible scenario for which the model has been determined.

Calibration. Simple calibration scenarios S_c are first considered for which laboratory experiments can be run that provide observables represented by data D_c. One then needs to:

1) introduce the likelihood pdf $\pi(D_c|\theta)$ for the calibration scenario based on the theory represented by (2.1),

2) provide the prior pdf $\pi_c(\theta)$,

3) solve the inverse problem for the posterior pdf σ_c using Bayes' Theorem, i.e.

$$\sigma_c(\theta) \propto \frac{\pi_c(\theta)\pi(D_c|\theta)}{\pi(D_c)} \tag{2.2}$$

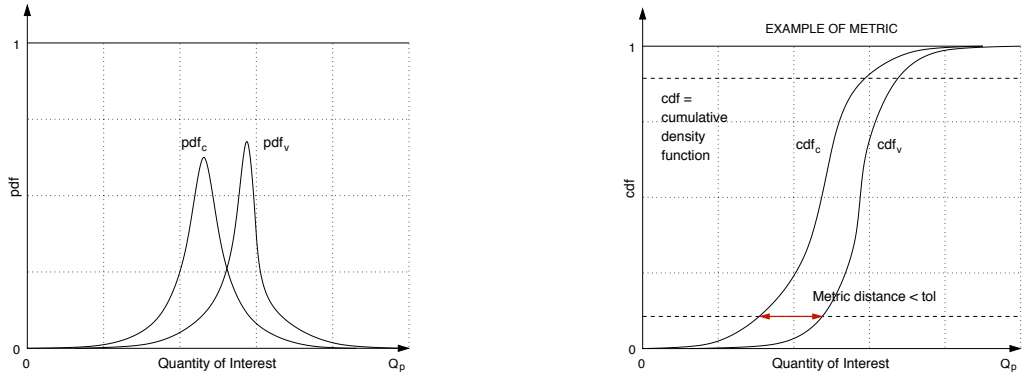

(a) Probability density functions (b) Cumulative distribution functions

FIGURE 2. Illustration of the metric $\mathcal{D}$ defined in (2.5).

using sampling methods such as those described in Cheung & Beck (2008).

4) solve the forward problem (2.1) for $u(\sigma_c(\theta), S_p)$ on the prediction scenario S_p, such that $\mathcal{A}\left(\sigma_c(\theta), S_p, u(\sigma_c(\theta), S_p)\right) = 0$ and predict the pdf $\pi^c(Q_p) = Q_p(u(\sigma_c(\theta), S_p))$.

Validation. A validation scenario S_v is now selected, usually with the objective of checking one or more hypotheses of the theory. Experiments are then conducted that produce validation observations. One may also hope that these observations will reflect the ability of the model to deliver acceptable predictions of the QoI Q_p. The procedure to compute $\pi^v(Q_p) = Q_p(u(\sigma_v(\theta), S_p)$ is similar as that described above.

Note that the mathematical model chosen for the prediction can never be validated. It can, at best, be not invalidated for the specific validation experiments we performed. The determination of a criterion for accepting a model as "not-invalidated" is a subjective decision that requires the acceptance of a metric to compare QoI's predicted in the calibration and the validation processes, and a tolerance that we establish as an acceptable measure of the predictability of the model. Thus, our validation process involves comparing $Q_p(u(\sigma_c(\theta), S_p))$ and $Q_p(u(\sigma_v(\theta), S_p))$. Let $\mathcal{D}$ denote a metric on the space of random functions containing $\pi^c(Q_p)$ and $\pi^v(Qp)$ and let γ_{tol} denote a preset tolerance. We will declare the model not-invalid if

$$\mathcal{D}\left(\pi^c(Q_p), \pi^v(Q_p)\right) < \gamma_{tol} \tag{2.3}$$

There are many metrics that could be used in (2.3). For example, computing the cumulative distribution functions (cdf's)

$$\mathrm{cdf}_c(Q_p) = \int_{-\infty}^{Q_p} \pi^c(Q)dQ \qquad \text{and} \qquad \mathrm{cdf}_v(Q_p) = \int_{-\infty}^{Q_p} \pi^v(Q)dQ \tag{2.4}$$

a comparison of $\pi^c(Q_p)$ and $\pi^c(Q_p)$ is then afforded by

$$\mathcal{D}\left(\pi^c(Q_p), \pi^v(Q_p)\right) = \sup_{p\in[0.1,0.9]} |\mathrm{cdf}_c^{-1} - \mathrm{cdf}_v^{-1}| \tag{2.5}$$

Such a metric is illustrated in Fig. 2.

The QoI chosen in this investigation is the radiative heating as it has a strong influence on the recession rate. The estimation of this quantity requires the knowledge of the spectral intensity, which is obtained at every point, for each propagation direction $\mathbf{s}$ and each wavelength λ, by solving the radiative transfer equation (RTE): $J'_\lambda(\mathbf{s}) = j_\lambda - \kappa_\lambda J_\lambda(\mathbf{s})$.

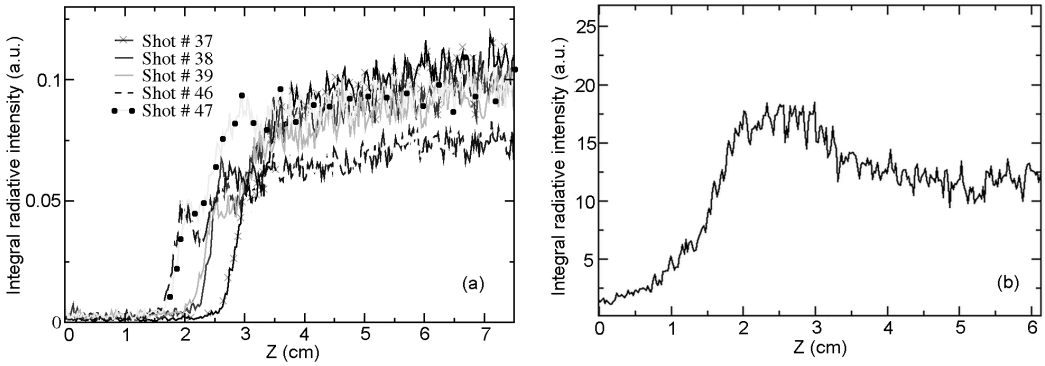

FIGURE 3. Spectrally integrated radiance versus distance along the shock-tube access. The spectral integration interval is 772–782 [nm]. (a) calibration data and (b) validation data (from Cruden *et al.* (2009)).

This equation has been written assuming that scattering by possible solid particles is negligible, since otherwise, the propagation directions would be coupled by this phenomenon. Also, the assumption of one-dimensional geometry adopted for the description of the flowfield inside the shock tube is retained in the solution of the radiative transfer problem which is readily solved using the discrete transfer method. Thus, the radiative flux on a surface can be easily calculated from the intensity following:

$$\mathbf{q_r} = \int_0^\infty \int_{4\pi} (\eta_\lambda - \kappa_\lambda J_\lambda(\mathbf{s}))\, d\lambda d\theta \tag{2.6}$$

3. Physical Models and Model Parameters

The one-dimensional shock-fitting Euler code SHOCKING and the MUTATION chemistry library are used to simulate the EAST flow field by solving the Rankine-Hugoniot jump equations to determine the post-shock conditions – i.e. by solving the conservation equations for mass, momentum, and global energy across the shock following Magin *et al.* (2006) and Panesi *et al.* (2009). Following the derivation of Thivet, the system of partial differential equations is first transformed into a system of ordinary differential equations that can be easily solved by means of the LSODE library (see Radhakrishnan & Hindmarsh (1993)). The code HPC-RAD computes the air plasma radiance based on the shock-layer thermochemistry predicted by SHOCKING. A detailed description of the models is given in Miki *et al.* (2010) and the model parameters that need to be calibrated are collected in Table 3. As indicated in this table, the shock speed and shock location are treated as uncertain parameters in the current study. Shock layer radiance significantly depends on the relative inflow velocity – e.g. in the limit of an optically thin shock layer plasma, the radiation intensity has an 8th-power dependence on the relative velocity. In the radiation model, we assume that all model parameters are well-defined considering the fact that oxygen $^5\mathrm{S}^0$-$^5\mathrm{P}$ transition at $\lambda_{\mathrm{lu}} = 777.55$ [nm] is a well-investigated line.

4. Description of Experimental Data

Data acquired during recent testing campaigns (series 46 and 47) at the NASA Ames EAST facility were used to calibrate the model parameters summarized in Table 3. Shock

Name	Symbol	$\pi(\theta)$
Normalized Inflow velocity	$u_i/\bar{u}_{o,i}$ (i=1-5)	$U[0.95, 1.05]$
Shock location	$L_{s,i}$ (i=1-5)	$U[-0.03, -0.01]$
Vib./Elec. coupling	r_i (i=1-2)	$U[0, 1.0]$
Electron energy removal rate	Ω_i (i=1-2)	$U[0, 1.0]$
Vib./Elec. Temp. at BC	$T_{v,o}$	$U[300, 10000.0]$
Chem. Reaction rate coff.	$log(A_i)$ (i=R1-R5)	$U[\bar{A} - 2, \bar{A} + 2]$
Chem. Reaction rate coff.	m_i (i=R1-R5)	$U[\bar{m} - 2, \bar{m} + 2]$
Chem. Reaction rate coff.	$\Theta_i/\bar{\Theta}_{0,i}$ (i=R1-R5)	$U[0.7, 1.3]$
Variance	σ^2	$U[0, (log(0.3)/2)^2]$

TABLE 1. List of uncertain parameters and prior distributions ($\pi(\theta)$). The forward reaction rates in Park's model are calculated with the modified Arrhenius equation, $k_{f,r} = 10^{A_r} T^{m_r} \exp(-\Theta_r/T)$. A sensitivity analysis was performed in order to identify the five reactions as having the largest impact on shock-heated air radiation calculations Miki *et al.* (2010): $R1 : N + e^- \leftrightarrow N^+ + 2e^-$, $R2 : N_2 + N \leftrightarrow 2N + N$, $R3 : N_2 + N_2 \leftrightarrow 2N + N_2$, $R3 : N_2 + e^- \leftrightarrow 2N + e^-$ and $R5 : O + e^- \leftrightarrow O^+ + 2e^-$.

	Calibration data					Validation data	Prediction data
Shot #	37	38	39	46	47	25	-
u_{in} [km/s]	10.26	10.00	10.03	9.94	10.25	9.88	11.50
P_{in} [Torr]	0.2	0.2	0.2	0.2	0.2	0.1	0.2

TABLE 2. Scenario parameters (EAST shock-tube experiments by Cruden *et al.* (2009)) are treated deterministically in the current study. For all cases, the inflow temperature is 300°K.

speeds in those experiments were approximately 10 [km/s] with tube pressures of 0.2 [Torr] (for the calibration data shown in Fig. 3 (a)) and 0.1 [Torr] (for the validation data shown in Fig. 3 (b)). Test conditions are summarized in Table 2. These represent typical conditions at the predicted peak heating point along the CEV lunar return trajectory. Details of the EAST facility and a discussion of some recent measurements commissioned by the NASA CAP can be found in Cruden *et al.* (2009).

5. Results and Discussion

The experimental data (e.g. Fig. 3) is composed of N_{exp} experiments, with $N_{\text{exp}} = 5$ for calibration and $N_{\text{exp}} = 6$ for validation. Each experiment supplies the same number N_d of data points. All data points are assumed to be statistically independent of each other. In the following discussion, we denote by $D_{i,j}$ the j^{th} data point of the i^{th} experiment, and by $X_{i,j}$ the corresponding computed model output. We also consider a multiplicative error, so that the numerically computed intensity is always of the same sign as that of

Inflow velocity

Model	$u_{37}/u_{37,\mathrm{o}}$	$u_{38}/u_{38,\mathrm{o}}$	$u_{39}/u_{39,\mathrm{o}}$	$u_{46}/u_{46,\mathrm{o}}$	$u_{47}/u_{47,\mathrm{o}}$	$u_{25}/u_{25,\mathrm{o}}$
1T (cal.)	0.998	1.045	1.036	1.048	0.998	-
1T (val.)	1.006	1.010	1.027	1.007	1.038	1.006
2T (cal.)	0.978	1.029	0.999	1.020	1.003	-
2T (val.)	0.994	1.025	0.975	1.015	1.012	0.969

Chemical reaction rates: $AT^m \exp(-\Theta/T)$

Model	$\frac{\log(A_{\mathrm{R1}})}{\log(A_{\mathrm{R1,o}})}$	$\frac{\log(A_{\mathrm{R2}})}{\log(A_{\mathrm{R2,o}})}$	$\frac{\log(A_{\mathrm{R3}})}{\log(A_{\mathrm{R3,o}})}$	$\frac{\log(A_{\mathrm{R4}})}{\log(A_{\mathrm{R4,o}})}$	$\frac{\log(A_{\mathrm{R5}})}{\log(A_{\mathrm{R5,o}})}$	-
1T (cal.)	0.902	0.958	1.073	1.096	1.092	-
1T (val.)	0.940	0.948	1.056	1.017	0.988	-
2T (cal.)	0.895	1.056	0.881	0.864	1.059	-
2T (val.)	0.890	1.000	1.003	0.944	1.037	-

Thermo. Transfer Coeff.

Model	r_1	r_2	Ω_1	Ω_2	$T_{o,v}/5000$	-
2T (cal.)	0.697	0.824	0.294	0.829	0.721	-
2T (val.)	0.272	0.340	0.394	0.592	1.352	-
	0.500	0.500	0.300	0.300	-	-

TABLE 3. Examples of statistics of model parameters. Lower subscript, o, indicates either the reference value or the reported value.

the data (i.e. positive): $D_{i,j} = X_{i,j}\exp(r_{\mathrm{total}})$, where r_{total} is a random variable. The pdf of r_{total} is chosen to be Gaussian with zero mean and variance σ^2. Based on these assumptions, the likelihood function becomes

$$\pi(D|\theta) = \frac{1}{(2\pi\sigma^2)^{(N_{\mathrm{exp}}N_d)/2}} \exp\left[-\frac{1}{2\sigma^2}\sum_{i=1}^{N_{\mathrm{exp}}}\sum_{j=1}^{N_d}(\tilde{D}_{i,j}-\tilde{X}_{i,j})^2\right] \tag{5.1}$$

where $\tilde{D}_{i,j} = \ln(D_{i,j}/D_{i,\mathrm{eq}})$ and $\tilde{X}_{i,j} = \ln(X_{i,j}/X_{i,\mathrm{eq}})$. Since there is a large uncertainty in the measurement of the inflow velocity, the radiance is normalized by the equilibrium values, $D_{i,\mathrm{eq}}$ and $X_{i,\mathrm{eq}}$. Using the Hybrid Gibbs Transitional Markov Chain Monte Carlo method proposed by Cheung & Beck (2008), and the parallel MPI/C++ statistical library QUESO Prudencio & Schulz (2011), we compute the solution to (2.2) to obtain the *posterior* pdf's of the aforementioned model parameters.

5.1. *Calibration of model parameters: Inverse problem*

We show in Table 3 the mean values of the model parameters after calibration (results of the shock locations are not reported here). We observe that the estimated shock velocities are slightly larger than the reference values by $\sim 1-3\%$ in most cases except for shot #37. The largest discrepancy among the two models is actually observed for shots #39 and

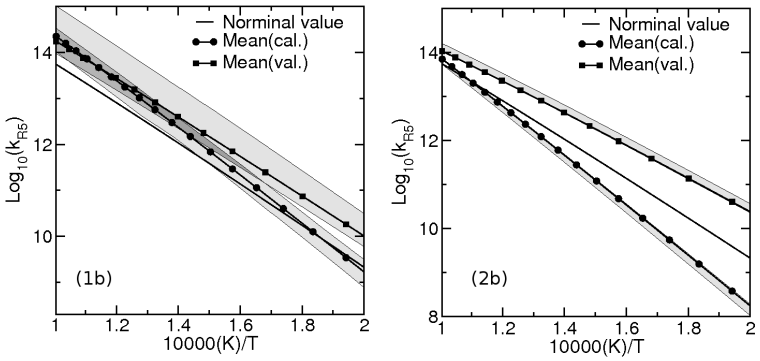

FIGURE 4. Posterior mean and 95% confidence interval (CI) for the log reaction rates (k_{R5}) versus $10^4(K)/T$. Results from the one-temperature model and from the two-temperature model are shown on the left plot and on the right plot, respectively. The gray region represents the 95% confidence interval.

#25. Recalling that the one-temperature model gives a peak value immediately behind the shock front, the quantified uncertainty in the inflow velocity should be different from that of the two-temperature model. As already mentioned, the shock speed is a critical parameter to the prediction of shock layer radiance.

As far as the five reactions considered in this study are concerned, the difference between the estimated values for the pertinent parameters (e.g. the Arrhenius coefficients) and those suggested by Park are within $\pm 15\%$ for the pre-exponential Arrhenius parameter A_i, $\pm 20\%$ for m_i, and $\pm 25\%$ for Θ_i. It is unclear, in view of the results, what the effects of the non-linear dependence of these parameters are on the reaction rates. For both models, the reaction rate R1 (ionization of the atomic nitrogen) is significantly suppressed. The delay in ionization results in the increase of the concentration of the atomic nitrogen, and thus dissociation of the nitrogen molecule by the atomic nitrogen is enhanced through the reaction R2. For the one-temperature model, the reaction rate R2 (dissociation of nitrogen molecule) is greatly overestimated so that the chemical energy takes the thermal energy out.As a result, it suppresses the unrealistic peak of the shock layer radiance behind the shock front. The predicted rates for R5, as shown in Figs. 4 (1a) and (1b), are relatively close to the nominal value for both models. Note that the vibration-dissociation coupling term r implicitly influences these rates for the two-temperature model, so that it is virtually impossible to isolate the uncertainties between the chemical kinetics parameters. It is also important to note that the location of the shock front also significantly influences the estimation of the reaction rates and corresponding uncertainties.

Referring to Table 3, we find that the estimated vibration-dissociation coupling terms r_1 (N_2) and r_2 (O_2) obtained from the calibration process are much larger than the ones computed from the re-calibration process. Note that their value is conventionally referenced as 0.5. A physical explanation for this trend could be hypothesized as follows: the validation data appears to indicate a more non-equilibrium thermo-chemical behavior when compared to the one from the calibration data due to the lower inflow pressure condition where Park's model fails. The coefficients used to describe the vibrational energy removal due to molecular dissociation were estimated to be $\Omega_1 \sim 0.3 - 0.4$ for N_2 and $\Omega_2 \sim 0.6 - 0.8$ for O_2. The reference value being 0.3, the larger value of Ω_2 can also be attributed to the fact that the current model overestimates the radiation

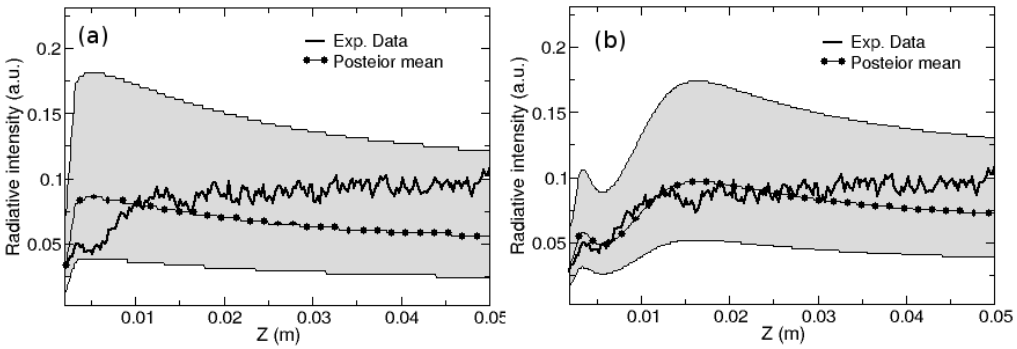

FIGURE 5. Predicted radiation intensity integrated over 772–782 [nm] (a) one-temperature model and (b) two-temperature model. For both cases, the scenario is the same as shot #47 reported in Table 1. The gray region denotes the 95% confidence interval (CI).

intensities in non-LTE regions; it is thus necessary to reduce T_v. The uncertain model parameter considered in the current model related to the boundary condition of T_v is shown in the last column of Table 3. No reference value is available. The larger value from the validation process is attributed to the calibrated shock location where the radiation intensity is different from zero and from where it immediately increases.

To simply verify that the statistical calculations performed with the proposed stochastic model are reasonable, we solve the forward problem in order to propagate the model parameter uncertainties (i.e., the posterior pdf's) onto the spectrally integrated shock layer radiance. The predicted radiation intensities using the one-temperature and the two-temperature models, integrated over the range 772–782 [nm] and corresponding to shot #47, are shown in Fig. 5. We can see that the experimental data lies within the 95 % CI for the both models and that it is very close to the posterior mean for the two-temperature model. As mentioned above, the one-temperature model has the maximum value immediately behind the shock front and is thus unable to capture the local peak seen near 0.005 [m]. On the other hand, the two-temperature model can reproduce such a non-equilibrium feature even if the profile does not reach the equilibrium state due to the delayed ionization process.

5.2. *Forward problem*

The QoI is chosen as the radiative heat flux in the stream-wise direction. Figure 6 shows the pdf's and cdf's of the QoI for the one-temperature model and the two-temperature model. For the former, the pdf of the QoI from the calibration process has a large variance and the peak shifts toward a smaller value following re-calibration. As a result, a large discrepancy between the two cdf's is observed ($\sim 84\%$). On the other hand, we observe in Fig. 6 that the results are better in the case of the two-temperature model. Indeed, the peak values stay relatively close to each other and the variance of the two pdf's remain unchanged. However, the discrepancy between the two cdf's is still fairly large. This unsatisfactory result for the two-temperature model, although commonly used in the hypersonic community, can be attributed to the fact that the Boltzmann distribution is used to model the internal energy state populations of a gas in both the LTE and non-

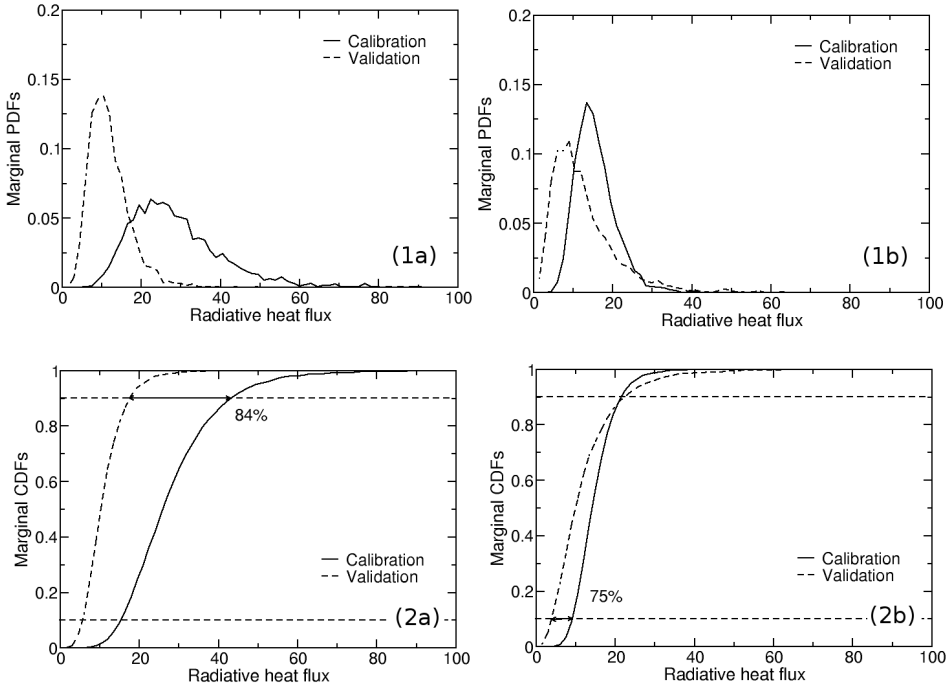

FIGURE 6. Probability density functions (upper row) and cumulative distribution functions (bottom row) for the radiative heat flux.

LTE regions. This assumption may not hold for the low-pressure inflow conditions as suggested by Johnston (2008).

6. Conclusion

A one- and a two-temperature thermochemical models were subjected to a validation process involving a statistical inverse problem, a statistical forward problem, one-dimensional shock-tube simulations, and experimental data from EAST. A total of 29-33 random model parameters were involved in the study and posterior pdf's for each parameter were computed through a Bayesian approach. The small variances in the pdf's of the model parameters indicate that there was a sufficient amount of experimental data to characterize each model parameter. Obviously, these pdf's are conditional on the physical model and the available experimental data. We also verified our probabilistic calculations by checking the consistency of our predictions against the experimental data. The validation process revealed that both thermochemical models should be considered invalid due to unacceptable large discrepancies observed in the QoI cdf's. The two-temperature model, though, showed better results than the one-temperature model, and we note that it is widely accepted by the supersonic communities. A possible improvement of this model could be achieved by relaxing the Boltzmann distribution assumption for the inner states of the populations. This will be the topic of future research work.

Acknowledgments. Material presented in this report is based upon work supported by the

Department of Energy (National Nuclear Security Administration) under Award Number DE-FC52-08NA28615. The authors would like to thank Profs. Moin and Iaccarino for offering the opportunity to work at CTR. Our thanks also go to Profs. Moser, Varghese, and Magin, as well as Drs. Cheung, Jagodzinski, and Brandis, for partial support and very fruitful discussions.

REFERENCES

Babuška, I., Nobile, F. & Tempone, F. 2008 A systematic approach to model validation based on Bayesian updates and prediction related rejection criteria. *Comput. Methods Appl. Mech. Engrg.* **197**, 2517–2539.

Cheung, S. H. & Beck, J. L. 2008 *New Bayesian updating methodology for model validation and robust predictions based on data from hierarchical subsystem tests*. EERL Report No. 2008-04, California Institute of Technology.

Cruden, B. A., Martinez, R., Grinstead, J. H. & Olejniczak, J. 2009 Simulation vacuum ultraviolet through near ir absolute radiation measurement with spatiotemporal resolution in an elesctric arc shock tube. In *AIAA*, pp. AIAA 2009–4240. San Antonio, Texas.

Johnston, C. 2008 A comparison of the east shock-tube data with a new air radiation model. In *AIAA*, pp. AIAA 2008–1245. Reno, Nevada.

Magin, T. E., L., Caillault., Bourdon, A. & Laux, C. O. 2006 Nonequilibrium radiative heat flux modeling for the huygens entry probe. *Journal of Geophysical Research* **111**, E07S12.

Miki, K., Panesi, M., Prudencio, E., Maurente, A., Goldstein, D., Jagodzunski, J., Prudhomme, S., Schulz, K., Simmon, C., Strand, J. & Varghese, P. 2010 On the (in)validation of a thermochemical model with east shock tube radiation measurements. In *AIAA*, pp. AIAA 2010–1557. Orlando, FL.

Panesi, M., Magin, T. E., Bourdon, A., Bultel, A. & Chazot, O. 2009 Fire 2 flight experiment analysis by means of a collisional-radiative model. *Journal of Thermophysics and Heat Transfer* **23**, 236–248.

Prudencio, Ernesto E. & Schulz, Karl W. 2011 The Parallel C++ Statistical Library 'QUESO': Quantification of Uncertainty for Estimation, Simulation and Optimization. *Submitted to IEEE IPDPS* .

Radhakrishnan, K. & Hindmarsh, A.C. 1993 Description and use of LSODE the livermore solver for ordinary differential equations. *NASA reference publication* **1**, 124.